

# Focusing Vacuum Fluctuations II

L.H. Ford<sup>1</sup>

Institute of Cosmology, Department of Physics and Astronomy  
Tufts University  
Medford, Massachusetts 02155

N.F. Svaiter<sup>2</sup>

Center for Theoretical Physics  
Laboratory for Nuclear Science and Department of Physics  
Massachusetts Institute of Technology  
Cambridge, Massachusetts 02139

## Abstract

The quantization of the scalar and electromagnetic fields in the presence of a parabolic mirror is further developed in the context of a geometric optics approximation. We calculate the mean squared scalar and electric fields near the focal line of a parabolic cylindrical mirror. These quantities are found to grow as inverse powers of the distance from the focus. We give a combination of analytic and numerical results for the mean squared fields. In particular, we find that the mean squared electric field can be either negative or positive, depending upon the choice of parameters. The case of a negative mean squared electric field corresponds to a repulsive Van der Waals force on an atom near the focus, and to a region of negative energy density. Similarly, a positive value corresponds to an attractive force and a possibility of atom trapping in the vicinity of the focus.

PACS categories: 03.70.+k, 34.20.Cf, 12.20.Ds, 04.62.+v.

## 1 Introduction

In a previous paper [1], henceforth I, we developed a geometric optics approach to the quantization of scalar and electromagnetic fields near the focus of a parabolic

---

<sup>1</sup>email: ford@cosm.phy.tufts.edu

<sup>2</sup>email: svaiter@lnsm.it.edu; Permanent address: Centro Brasileiro de Pesquisas Físicas CBPF, Rua Dr. Xavier Sigaud 150, Rio de Janeiro, RJ, 22290-180, Brazil

mirror. We found that there can be enhanced fluctuations near the focus in the sense that mean squared field quantities scale as an inverse power of the distance from the focus, rather than an inverse power of the distance from the mirror. These enhanced fluctuations were found to arise from an interference term between different reflected rays. In the present paper we extend the previous treatment. In I, only points on the symmetry axis were considered. Here we are able to treat points in an arbitrary direction from the focal line of a parabolic cylinder. We give more detailed numerical results which provide a fuller picture of the phenomenon of focusing of vacuum fluctuations. We also correct some erroneous results in Sect. V of I.

The outline of the present paper is as follows: In Sect. 2, we review and extend some of the formalism used to calculate the mean squared scalar and electric fields,  $\langle \phi^2 \rangle$  and  $\langle E^2 \rangle$ , near the focus. In Sect. 3 we derive some geometric expressions which are needed to study fluctuations at points off of the symmetry axis. In Sect. 4, the evaluation of integrals with singular integrands is revisited. Two different, but equivalent, approaches are discussed. A particular case where the integrals can be performed analytically is examined in Sect. 5. More generally, it is necessary to calculate  $\langle \phi^2 \rangle$  and  $\langle E^2 \rangle$  numerically. A procedure for doing so is outlined in Sect. 6. Some detailed numerical results are also presented there. The limits of validity of our model and results will be examined in Sect. 7. This discussion will draw on some results on diffraction obtained in the Appendix. The experimental testability of our conclusions will be discussed in Sect. 8. Finally, the results of the paper will be summarized in Sect. 9.

Units in which  $\hbar = c = 1$  will be used throughout this paper. Electromagnetic quantities will be in Lorentz-Heaviside units.

## 2 Basic Formalism

Here we will briefly review the geometric optics approach developed in I. The basic assumption is that we may use a ray tracing method to determine the functional form of the high frequency modes, which will in turn give the dominant contribution to the expectation values of squared field operators. We start with a basis of plane wave modes. The incident wave, for a scalar field, may be taken to be

$$f_k = \frac{1}{\sqrt{2V}} e^{i(k \cdot x - \omega t)}; \quad (1)$$

with box normalization in a volume  $V$ . In the presence of a boundary, this is replaced by the sum of incident and reflected waves,

$$F_k = f_k + \sum_i f_k^{(i)}; \quad (2)$$

where the  $f_k^{(i)}$  are the various reflected waves. One could also in principle adopt a wavepacket basis, in which  $F_k$  is replaced by a localized wavepacket. Because the time

evolution preserves the Klein-Gordon norm, if the various modes are orthonormal in the past, they will remain so after reflection from the mirror. Thus we can view Eq. (2) as the limit of a set of orthonormal wavepacket modes in which the modes become sharply peaked in frequency and hence delocalized.

It was shown in I that the renormalized expectation value of the squared scalar field is given by a sum of interference terms:

$$\langle \phi^2 \rangle = \sum_k \sum_i \frac{1}{4} (f_k^{(i)} f_k^{(i)} + f_k f_k^{(i)}) + \sum_{i \neq j} f_k^{(i)} f_k^{(j)} \quad (3)$$

This renormalized expectation value is defined as a difference in the mean value of  $\phi^2$  with and without the mirror, and hence will vanish at large distances from the mirror. The various interference terms in the above expression yield contributions to  $\langle \phi^2 \rangle$  which are proportional to the inverse square of the appropriate path difference. Thus in the vicinity of the focus, the interference terms between different reflected rays will dominate over that between the incident and a reflected ray. In the present paper, we will consider cases with no more than two reflected rays, and write

$$\langle \phi^2 \rangle = 2 \operatorname{Re} \sum_k f_k^{(1)} f_k^{(2)} \quad (4)$$

In the case of a parabolic cylinder, this may be expressed as

$$\langle \phi^2 \rangle = \frac{1}{3^2} \int \frac{d^0}{(\Delta)^2} \quad (5)$$

Here  $\Delta$  is the path difference for the two reflected rays, and the integration is over the reflection angle of one of the rays. The range is chosen so that each pair of reflected rays is counted once. The corresponding expression for the mean squared electric field near the focus of a parabolic cylinder is found in I to be

$$\langle E^2 \rangle = \frac{8}{5^3} \int \frac{d^0}{(\Delta)^4} \quad (6)$$

### 3 Optics of Parabolic Mirrors

In this section, we wish to generalize some of the results of I concerning the incident and reflected rays in the presence of a parabolic mirror. Consider the geometry illustrated in Fig. 1. An incident ray at an angle  $\theta$  to the symmetry axis is reflected from the point  $(x_i, y_i)$ , and then reaches the point P at an angle of  $\theta^0$ . We first need to find the relation between  $\theta$  and  $\theta^0$ . Note that the reflected ray crosses the symmetry axis at a distance  $c$  from the focus. It was shown in I that

$$c = \frac{c \sin^3 \theta^0}{b(1 - \cos \theta^0)} \quad (7)$$

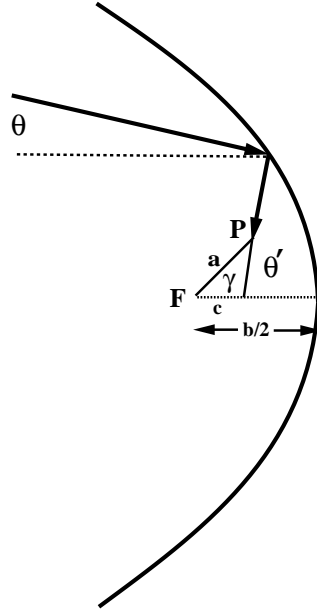


Figure 1: An incident ray at an angle  $\theta$  reflects off of a parabolic mirror at an angle  $\theta'$  and arrives at the point of interest  $P$ . This point is a distance  $a$  from the focus  $F$  in a direction at an angle  $\gamma$  with respect to the symmetry axis. Throughout this paper, we assume that  $a < b$ , where  $\frac{1}{2}b$  is the distance from the focus to the mirror.

However, from the law of sines, we have that

$$c \sin \theta = a \sin(\theta - \gamma) \quad (8)$$

Hence we now have that

$$f(\theta) = \frac{a}{b} \sin(\theta - \gamma) \quad (9)$$

where

$$f(\theta) = \frac{\sin^3 \theta \sin(\theta - \gamma)}{(1 - \cos \theta)} \quad (10)$$

There will be multiple reflected rays whenever different values of  $\theta'$  are associated with the same value of  $f$ . The function  $f(\theta)$  is plotted in Fig. 2 for various values of  $\gamma$ . We can see from these plots that in general there can be up to four reflected angles  $\theta'$  for a given incident angle  $\theta$ . However, if the mirror size  $\theta_0$  is restricted to be less than  $2\pi/3$ , then there will never be more than two values of  $\theta'$  for a given  $\theta$ . Throughout this paper, we will assume  $\theta_0 < 2\pi/3$ , and hence have at most two reflected rays for a given incident ray. The two reflected rays will occur at  $\theta' = \theta_1$  and  $\theta' = \theta_2$ , where

$$f(\theta_1) = f(\theta_2) \quad (11)$$

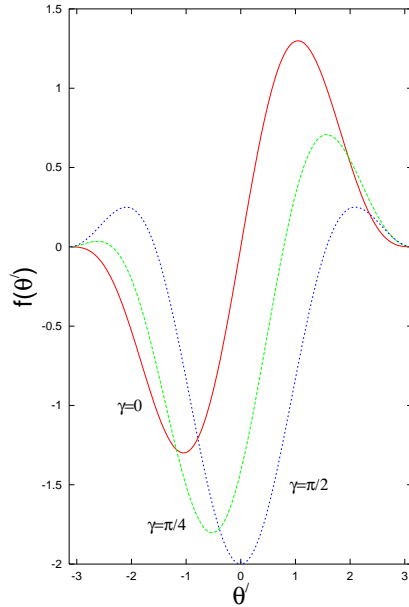


Figure 2: The function  $f(\theta)$  is plotted for various values of  $\gamma$ . This function relates the angle of the incident ray,  $\theta$ , to the angle of the reflected ray,  $\theta'$ , through the relation  $\theta' = (a/b) f(\theta)$ .

Our next task is to calculate the difference in path length,  $\Delta s$ , for these two reflected rays. Again, this is a generalization of a calculation given in I.C consider the situation illustrated in Fig. 3, where a reflected ray with angle  $\theta'$  reaches the point P after reflecting from the point  $(x_i; y_i)$  on the mirror. Let  $s_1$  be the distance traveled after reflection, and  $s_2$  be the distance traveled between when the ray crosses the line  $x = x_0$  and when it reaches the mirror. Note that

$$s_2 = (x_i - x_0) \sec \theta' = x_i - x_0 + O\left(\frac{a^2}{b^2}\right) \quad (12)$$

Even if  $x_i < 0$ , we can choose  $x_0$  to be such that  $s_2 > 0$ . Next note that

$$s_1 = (y_i - a \sin \theta') \csc \theta' \quad (13)$$

The reflection point  $(x_i; y_i)$  is the intersection of the line

$$y = \tan \theta' (x - a \cos \theta') + a \sin \theta' \quad (14)$$

with the parabola, given by

$$x = \frac{b^2 - y^2}{b} \quad (15)$$

These relations lead to

$$y_i = b \cot \theta' \sec \theta' \left[ 1 - 2 \frac{a}{b} \sin^2 \theta' (\cos \theta' \sin \theta' \cot \theta') \right] \quad (16)$$

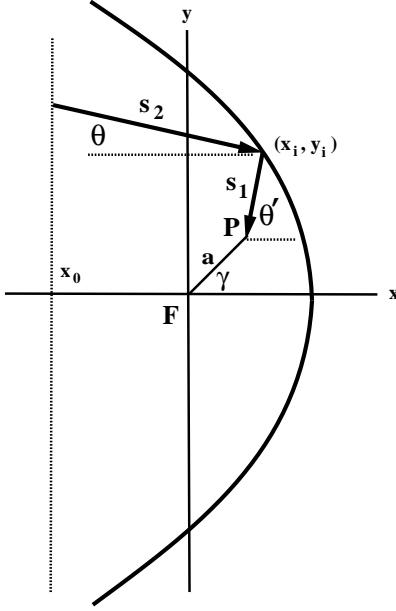


Figure 3: The distance travelled by a ray which reaches the point P is illustrated. Here the line  $x = x_0$  is an arbitrarily chosen vertical line somewhere to the left of the point of reflection. The incident ray travels a distance  $s_2$  from this line to the point of reflection. After reflection it travels a distance  $s_1$  before arriving at the point P. This point is a distance  $a$  from the focus F in a direction given by the angle  $\gamma$ .

We may now expand this expression to first order in  $a=b$  and combine it with our previous expressions to show that, to first order,

$$\Delta = s_1 + s_2 = b - x_0 - a(\cos \theta - \cos \theta') + \sin \theta - \sin \theta' : \quad (17)$$

Thus the magnitude of the path length difference for  $\theta$  and  $\theta'$ , two different values of  $\theta$ , is

$$\Delta = a[j\cos(\theta - \theta') + \sin(\theta - \theta')] : \quad (18)$$

In the limit that  $\theta - \theta' = 0$ , we obtain the result for  $\Delta$  used in I.

## 4 Evaluation of Singular Integrals

We can express Eq. (5) as

$$h^2 i = \frac{1}{6^2 a^2} \int \frac{d}{h^2} ; \quad (19)$$

and Eq. (6) as

$$hE^2 i = \frac{4}{5^3 a^4} \int \frac{d}{h^4} : \quad (20)$$

Here

$$h = h(\theta; \phi) = j \cos(\theta - \phi) + \sin(\theta) \sin(\phi); \quad (21)$$

and the integrations run over the full range for which there are two reflected rays, thus counting each pair twice.

The integrands of these integrals contain singularities within the range of integration. These singularities occur at a critical angle,  $\theta_c$ , at which  $h$  vanishes linearly. Thus the  $h^{-2}$  integral contains a  $(\theta - \theta_c)^{-2}$  singularity, and the  $hE^{-2}$  contain a  $(\theta - \theta_c)^{-4}$  singularity. These singularities are presumably artifacts of assuming perfect mirrors with sharp boundaries as will be discussed in Sect. 7. The singularity occurs when both  $\theta$  and  $\phi$  are approaching  $\theta_c$  from opposite directions. The critical angles  $\theta_c$  are just the extrema of the function  $f(\theta)$ .

Integrals with such singular integrands can be defined by a generalization of the principal value prescription. This generalization involves an integration by parts to recast the original integral as one containing a less singular integrand, plus surface terms. For example, we may use

$$\frac{1}{x^2} = \frac{1}{2} \frac{d^2}{dx^2} \ln x^2 \quad (22)$$

to write

$$\int_a^{Z_b} dx \frac{f(x)}{x^2} = \frac{1}{2} \int_a^{Z_b} dx f^{(0)}(x) \ln x^2 + \left[ \frac{f(x)}{x} + \frac{1}{2} f^{(0)}(x) \ln x^2 \right]_a^{Z_b} : \quad (23)$$

Similarly,

$$\frac{1}{x^4} = \frac{1}{12} \frac{d^4}{dx^4} \ln x^2 : \quad (24)$$

leads to

$$\int_a^{Z_b} dx \frac{f(x)}{x^4} = \left[ \frac{f(x)}{3x^3} + \frac{f^{(0)}(x)}{6x^2} + \frac{f^{(0)}(x)}{6x} + \frac{1}{12} f^{(0)}(x) \ln x^2 \right]_a^{Z_b} + \frac{1}{12} \int_a^{Z_b} dx \ln x^2 \frac{d^4 f(x)}{dx^4} : \quad (25)$$

If  $b > 0$  and  $a < 0$ , there were singularities in the original integrals which are replaced by integrable, logarithmic singularities. In all cases, the surface terms are evaluated away from the singularity and are hence finite.

If  $f$  and a sufficient number of its derivatives vanish at the endpoints, then the surface terms vanish. In I, it was incorrectly argued that the surface terms which arise in the present problem can be ignored. It is true that if the reflectivity of the mirror falls smoothly to zero, the surface terms vanish. However, in this case it would be necessary to integrate explicitly the function which is falling smoothly to zero. If the reflectivity falls very rapidly at the edge of the mirror, its derivatives will be large, and effectively reproduce the surface terms. Thus, the explicit results given in Sect. V of I are incorrect. In Sects. 5 and 6 of the present paper, we will give new results which replace and generalize the older results.

There is an alternative way to implement the above integration by parts prescription. This is simply to evaluate the integral as an indefinite integral, and evaluate the result at the endpoints, ignoring the singularity within the integration range. Even if it is not possible to find a closed form expression for the indefinite integral, one can expand the integrand in a Laurent series about  $x = 0$  and integrate term by term, using the relation

$$\int_a^b \frac{1}{x^n} dx = \frac{1}{n+1} \left[ \frac{1}{a^{n+1}} - \frac{1}{b^{n+1}} \right] \quad (26)$$

One can verify this relation for the case  $a < 0 < b$  using the above integration by parts method.

One peculiar feature is that both  $h'^2 i$  and  $hE^2 i$  will diverge for particular values of  $\theta_0$ . This arises when  $\theta_c$ , the extremum of  $f(\theta)$ , approaches the edge of the mirror,  $\theta_0 = \theta_c$ . The mathematical reason for the divergence is that one limit of integration is approaching a point at which  $h = 0$  and the integrand is singular. This corresponds to letting either  $a \rightarrow 0$  with  $b$  fixed, or  $b \rightarrow 0$  with  $a$  fixed, in Eq. (26). The physical origin of this singular behavior is that we have made two unrealistic assumptions. The mirror is assumed to be perfectly reflecting at all frequencies and to have sharp edges at  $\theta_0 = \theta_c$ . This will be discussed further in Sect. 7.

## 5 Exact Results for $\theta_c = \frac{\pi}{2}$

In general, the integrals for  $h'^2 i$  and  $hE^2 i$ , Eqs. (5) and (6), respectively, can only be evaluated numerically. This is in part because the second reflection angle  $\theta_2$  is implicitly given as a function of the first angle,  $\theta_1$ . There is one case in which this relation may be written down in closed form. This is when  $\theta_c = \frac{\pi}{2}$ , so the function  $f(\theta)$  is symmetrical about the origin. In this case, we have

$$\theta_2 = \pi - \theta_1 \quad (27)$$

and we can write

$$h'^2 i = \frac{1}{24 \sqrt{3} a^2} \int_0^{\theta_0} \frac{d\theta}{\sin^2 \theta} = \frac{\cot \theta_0}{12 \sqrt{3} a^2} \quad (28)$$

Similarly,

$$hE^2 i = \frac{1}{20 \sqrt{3} a^4} \int_0^{\theta_0} \frac{d\theta}{\sin^4 \theta} = \frac{\cos \theta_0 (3 - 2 \cos^2 \theta_0)}{30 \sqrt{3} a^4 \sin^3 \theta_0} \quad (29)$$

These expressions are plotted in Fig. 4. Note that both  $h'^2 i$  and  $hE^2 i$  can have either sign:

$$\begin{aligned} h'^2 i > 0 \quad \text{and} \quad hE^2 i < 0 \quad \text{for} \quad 0 < \theta_0 < \frac{\pi}{2}; \\ h'^2 i < 0 \quad \text{and} \quad hE^2 i > 0 \quad \text{for} \quad \frac{\pi}{2} < \theta_0 < \frac{2\pi}{3}; \end{aligned} \quad (30)$$



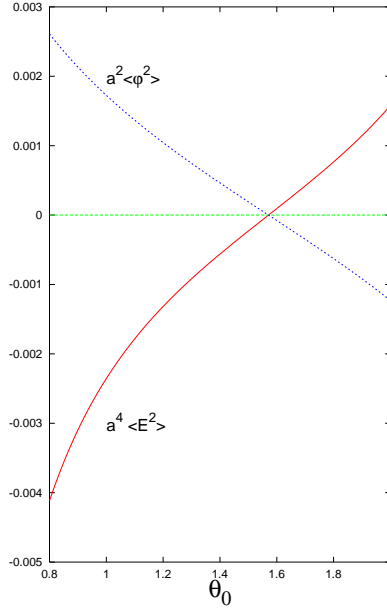


Figure 4: The exact solutions for  $\langle h'^2 \rangle$  and  $\langle hE^2 \rangle$  for the case that  $\theta = \frac{\pi}{2}$  are plotted as functions of the m error size.

Both quantities seem to diverge in the limit that  $\theta_0 \rightarrow 0$

$$\begin{aligned} \langle h'^2 \rangle & \sim \frac{1}{12 \theta_0^3 a^2} ; \\ \langle hE^2 \rangle & \sim \frac{1}{30 \theta_0^3 a^4} : \end{aligned} \quad (31)$$

This divergence is a special case of the singularities arising when the edge of the m error approaches an extremum of  $f(\theta)$ .

We can go further and find the derivatives of both  $\langle h'^2 \rangle$  and  $\langle hE^2 \rangle$  with respect to  $\theta_0$ , at  $\theta = \frac{\pi}{2}$ . First, we need to find  $f(\theta)$  to first order in  $\theta - \frac{\pi}{2}$ . We may expand the relation  $f(\theta) = f(\frac{\pi}{2})$  to this order and show that

$$f(\theta) = \frac{2 \sin^2(\theta - \frac{\pi}{2})}{(\cos \theta - 1)(2 \cos \theta + 1)} + \dots : \quad (32)$$

We can next expand  $1-h^2$  and  $1-h^4$  to first order in  $\theta - \frac{\pi}{2}$ . The first order corrections are odd functions of  $\theta$  whose explicit forms we will not need.

The crucial effect of varying  $\theta$  slightly away from  $\theta = \frac{\pi}{2}$  is to change the range of integration. First consider the case where  $\theta < \frac{\pi}{2}$ . The integration range now becomes

$$\theta_0 < \theta < \theta_0 ; \quad (33)$$

where

$$\theta_0 = \frac{2 \sin^2 \theta_0(\frac{\pi}{2} - \theta_0)}{(1 - \cos \theta_0)(2 \cos \theta_0 + 1)} : \quad (34)$$

To first order in  $\frac{z_0}{2}$ , we can write

$$h'^2 i = \frac{1}{6^3 a^2} \int_{-z_0}^{z_0} \frac{d}{h^2} \dots \#$$

$$= \frac{1}{6^3 a^2} \int_{-z_0}^{z_0} \frac{1}{h^2} + \dots \int_{-z_0}^{z_0} \frac{1}{h^2} \dots \int_{-z_0}^{z_0} \frac{1}{h^2} \dots \# ; (35)$$

where the subscripts on  $1=h^2$  denote the order in an expansion in powers of  $\frac{z_0}{2}$ . The first term on the right hand side of Eq. (35) is just the zeroth order part given by Eq. (28). The next term vanishes because  $(1=h^2)_1$  is an odd function. The final term may be approximated using

$$\int_{-z_0}^{z_0} \frac{1}{h^2} \dots \int_{-z_0}^{z_0} \frac{1}{h^2} \dots = \dots : (36)$$

This leads to

$$h'^2 i = \frac{1}{12^3 a^2} \frac{1}{\tan \theta_0} \frac{1}{(1 - \cos \theta_0)(2 \cos \theta_0 + 1)} + \dots \# ; \theta_0 < \frac{\pi}{2} : (37)$$

We may now repeat this procedure for  $\theta_0 > \frac{\pi}{2}$ . In this case, the range of integration is

$$-z_0 < \dots < z_0 ; (38)$$

and  $\theta_0 < 0$ , so the range of integration has again decreased. This causes the first order change in  $h'^2 i$  to have the same magnitude but the opposite sign from the previous case. Thus in all cases, we can write

$$h'^2 i = \frac{1}{12^3 a^2} \frac{1}{\tan \theta_0} \frac{1}{(1 - \cos \theta_0)(2 \cos \theta_0 + 1)} + \dots \# : (39)$$

A similar analysis may be applied to  $hE^2 i$  with the result

$$hE^2 i = \frac{4}{5^3 a^4} \frac{\cos \theta_0 (3 - 2 \cos^2 \theta_0)}{24 \sin^3 \theta_0} \frac{1}{8 \sin^2 \theta_0 (1 - \cos \theta_0)(2 \cos \theta_0 + 1)} + \dots \# : (40)$$

Thus both  $h'^2 i$  and  $hE^2 i$  have cusps at  $\theta_0 = \frac{\pi}{2}$ . The nonanalytic behavior is due to the fact that the range of integration decreases whenever  $\theta_0$  moves away from  $\frac{\pi}{2}$  in either direction. As will be discussed in Sect. 7, the cusp is presumably an artifact of a sharp edge approximation, and should be smoothed out in a more exact treatment.

## 6 Numerical Procedures and Results

Apart from the special cases discussed in the previous section, it is necessary to evaluate  $h'^2 i$  and  $hE^2 i$  numerically. The first step is to find the second reflection

angle  $\theta$  as a function of the first reflection angle  $\theta_0$ . This involves a straightforward numerical solution of the equation

$$f(\theta) = f(\theta_0) : \quad (41)$$

Because we assume a restriction on the angle size of the mirror,

$$\theta_0 < \frac{2}{3} \pi ; \quad (42)$$

there will always be either one or no roots for  $\theta$ . Within the geometric optics approximation that we use, integrands are assumed to vanish in regions where there are no roots.

As was discussed in Sect. 4, there are at least two methods that may be used for explicit evaluation of the integrals which appear in the geometric optics expressions for  $h^{(2)}i$  and  $hE^{(2)}i$ . The first is an integration by parts, which replaces the singularity in Eqs. (19) and (20) by a logarithmic singularity. Here we will outline how this may be done explicitly. Consider first Eq. (19), which may be expressed as

$$h^{(2)}i = \frac{1}{6^2 a^2} \int_{\theta_1}^{\theta_2} \frac{d}{[h(\theta; \theta_0)]^2} d\theta : \quad (43)$$

Suppose that we are interested in integrating over the range  $\theta_1 < \theta < \theta_2$  and that this range contains one point  $\theta = \theta_0$  at which  $h = 0$ . We can write

$$h^{(2)}i = \frac{1}{12^2 a^2} \int_{\theta_1}^{\theta_2} d\theta \frac{(\theta - \theta_0)^2}{[h(\theta; \theta_0)]^2} \frac{d^2}{d\theta^2} \log(\theta - \theta_0)^2 : \quad (44)$$

The quantity  $(\theta - \theta_0)^2/[h(\theta; \theta_0)]^2$  is finite at  $\theta = \theta_0$ . This expression may now be integrated by parts, as in Eq. (23). The derivatives of  $h$  which arise are computed using Eq. (21) and the relation

$$\frac{d}{d\theta} = \frac{f'(\theta)}{f(\theta)} : \quad (45)$$

An analogous procedure can be applied to  $hE^{(2)}i$ . The detailed expressions for  $h^{(2)}i$  and  $hE^{(2)}i$  which result from this procedure are rather complicated, and will not be written down explicitly.

The second method which may be employed is a variant of the direct integration illustrated in Eq. (26). The actual integrands in Eqs. (19) and (20) are too complex to integrate in closed form. However, we can use numerical integration of  $1/h^2$  and  $1/h^4$  in regions away from zeros of  $h$  and direct integration of a series expansion in the neighborhood of a zero. The first step in the generation of the series expansion is to expand  $(\theta - \theta_0)$  around  $\theta = \theta_0$ ,

$$(\theta - \theta_0) = 2\theta_0 + a_2(\theta - \theta_0)^2 + a_3(\theta - \theta_0)^3 + \dots : \quad (46)$$

The coefficients are found by inserting this expansion into Eq. (41) and then expanding both sides of the resulting expression in powers of  $\epsilon_0$ . A few of the leading coefficients are

$$\begin{aligned} a_2 &= \frac{f''''}{3f''} ; \\ a_3 &= \frac{(f''')^2}{9(f'')^2} ; \\ a_4 &= \frac{9(f'')^2 (f^{(5)})^2 - 30f''f''''f^{(4)} + 40(f''')^2}{540(f'')^3} ; \end{aligned} \quad (47)$$

where the derivatives of  $f$  are evaluated at  $x = x_0$ . The expansion for  $y(x)$  is then used to generate analogous expansions for  $l=h^2$  and  $l=h^4$ , which are in turn integrated over the interval  $x_0 - \epsilon_0 < x < x_0 + \epsilon_0$  using Eq. (26). The result is combined with the direct numerical integration outside of this interval. Here  $\epsilon_0$  is an arbitrary small positive number. One of the tests of the numerical procedure is the independence of the results upon the choice of  $\epsilon_0$ .

We have developed numerical routines based upon both of the above procedures. The plots which are given below were created using a routine based upon the second method, with an expansion of  $y$  to sixth order in  $\epsilon_0$ . The particular values of  $\epsilon_0$  were in the range  $0.1 \leq \epsilon_0 \leq 0.3$ . In this range, the routine is relatively stable and insensitive to  $\epsilon_0$ . Smaller values of  $\epsilon_0$  can lead to instability, as the contributions from  $|x - x_0| > \epsilon_0$  and from  $|x - x_0| < \epsilon_0$  are both large in magnitude and tending to cancel each other.

Numerical results for  $h'^2 i$  and  $hE^2 i$  for various values of  $\epsilon_0$  are shown in Figs. 5-12 as functions of  $\epsilon_0$ . In all cases, there are values of  $\epsilon_0$  at which  $h'^2 i$  or  $hE^2 i$  are singular in the model of a perfectly reflecting mirror with sharp edges. These points occur when an extremum of the function  $f(x)$  sits at an edge of the mirror,  $x_0 = x_0$ . The values and slopes of  $h'^2 i$  and  $hE^2 i$  at  $\epsilon_0 = \frac{1}{2}$  are in agreement with Eqs. (39) and (40). We can see from the graphs that for smaller mirrors,  $\epsilon_0 < \frac{1}{2}$ , we have  $h'^2 i > 0$  and  $hE^2 i < 0$  everywhere. For larger mirrors,  $\epsilon_0 > \frac{1}{2}$ , we have regions where  $h'^2 i > 0$  and other regions where it is negative, and similarly for  $hE^2 i$ . The signs of  $h'^2 i$  and of  $hE^2 i$  always seem to be opposite. The regions near  $\epsilon_0 = \frac{1}{2}$  for larger mirrors where  $hE^2 i > 0$  are of special interest. These are regions where an atom will feel an attractive force toward the focus, and thus has the possibility of being trapped.

## 7 Limits of Validity of the Results

In this section, we will discuss the likely ranges of validity of the model we have used to calculate  $h'^2 i$  and  $hE^2 i$ . In particular, we have assumed a geometric optics approximation, and a mirror which is both perfectly reflecting and has sharp edges. Each of these assumptions will be examined critically.

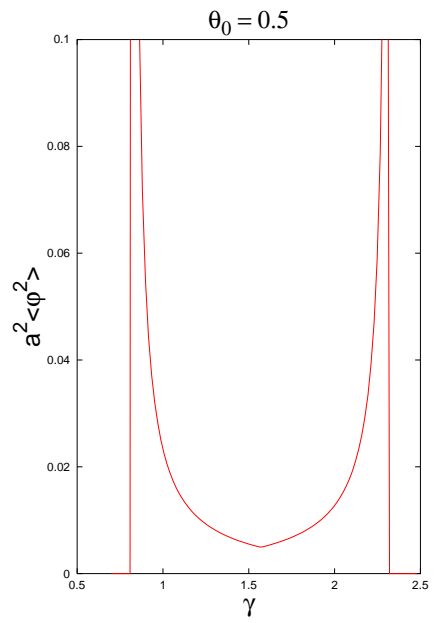


Figure 5:  $\langle a^2 \rangle_{\varphi^2}$  for  $\theta_0 = 0.5$ .

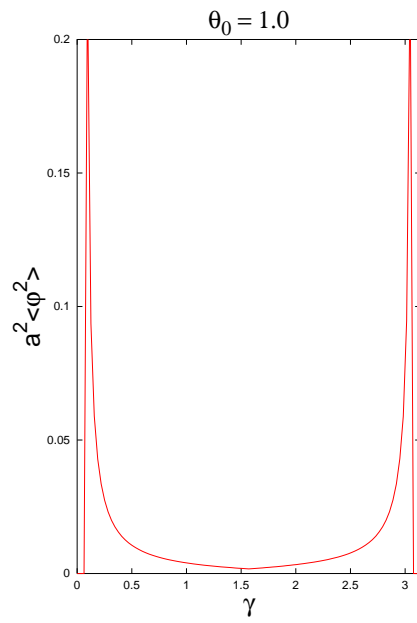


Figure 6:  $\langle a^2 \rangle_{\varphi^2}$  for  $\theta_0 = 1.0$ .

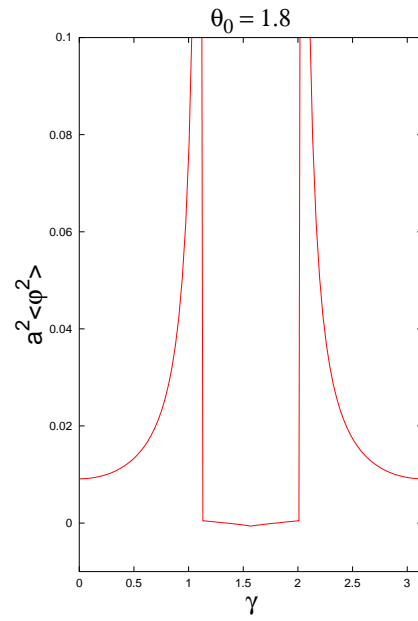


Figure 7:  $\langle a^2 \langle \phi^2 \rangle$  for  $\theta_0 = 1.8$ .

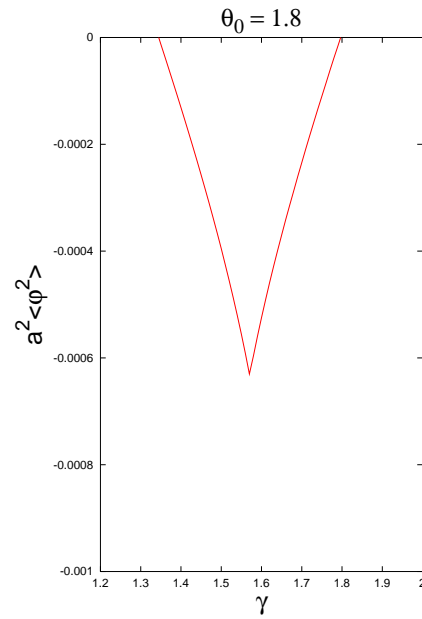


Figure 8:  $\langle a^2 \langle \phi^2 \rangle$  for  $\theta_0 = 1.8$ , showing in detail the region where  $\langle a^2 \langle \phi^2 \rangle < 0$ .

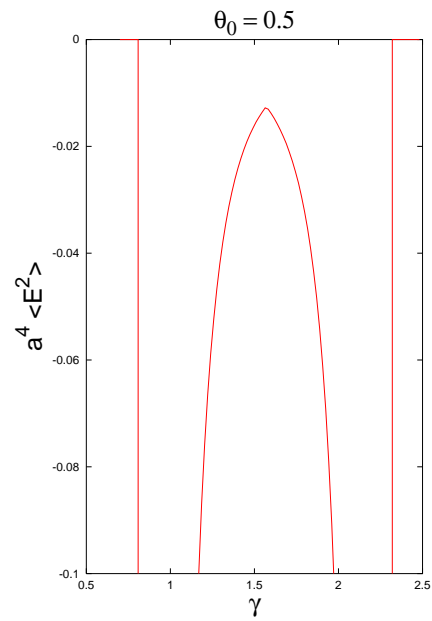


Figure 9:  $\langle E^2 \rangle$  for  $\theta_0 = 0.5$ .

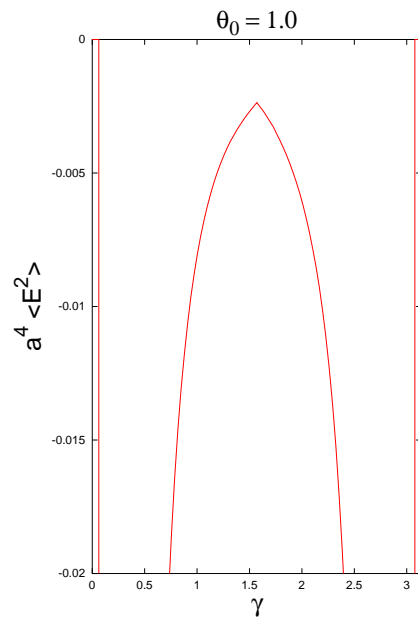


Figure 10:  $\langle E^2 \rangle$  for  $\theta_0 = 1.0$ .

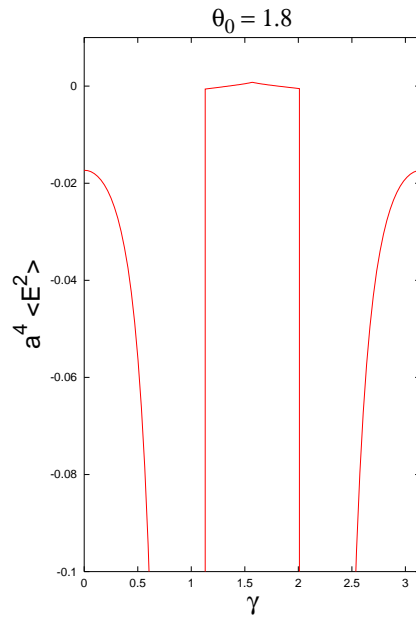


Figure 11:  $\langle E^2 \rangle$  for  $\theta_0 = 1.8$ .

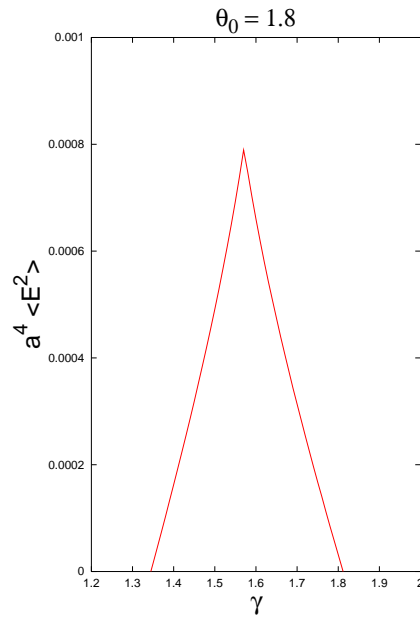


Figure 12:  $\langle E^2 \rangle$  for  $\theta_0 = 1.8$ , showing in detail the region where  $\langle E^2 \rangle > 0$ .



## 7.1 Geometric Optics

The use of geometric optics amounts to ignoring diffraction effects, so we can gauge the accuracy of geometric optics by estimating the size of these effects. In the geometric optics approximation, the incident and reflected waves in Eq. (2) all have the same magnitude. Suppose that we now introduce a correction due to diffraction and write

$$F_k = f_k + \sum_i f_k^{(i)} + F_k : \quad (48)$$

In the case of a plane strip which has width  $2y_0$  in one direction and is infinite in the other direction, the magnitude of the diffraction correction is estimated in the Appendix with the result  $|F_k - F_k| \approx y_0$ , where  $\lambda$  is the wavelength of the incident wave. In our case, we have a parabolic cylinder characterized by the length scale  $b$ . We could imagine representing the parabolic cylinder by a set of strips which are infinite in the  $z$ -direction. The order of magnitude of the diffraction correction should be the same as for a single strip of width  $b$ . Thus we estimate that in the present case

$$\frac{F_k}{F_k} \approx \frac{b}{\lambda} : \quad (49)$$

The wavelengths which give the dominant contribution to  $h^{-2}i$  and  $hE^{-2}i$  near the focus are those of order  $a$ . Thus the interference term between  $F_k$  and any of the other terms in Eq. (48) should yield contributions to  $h^{-2}i$  and  $hE^{-2}i$  which are smaller than the dominant contribution by a factor of the order of  $b/a$ . Thus we estimate the diffraction contribution to  $h^{-2}i$  to be of order

$$h^{-2}i \approx \frac{1}{a^{3/2} b^{1/2}} ; \quad (50)$$

and that to  $hE^{-2}i$  to be of order

$$hE^{-2}i \approx \frac{1}{a^{7/2} b^{1/2}} : \quad (51)$$

Note that the geometric optics results near the focus depend only upon  $a$  and  $\theta_0$ , the angular size of the mirror, but not upon  $b$ , the linear dimension of the mirror. However, the diffraction correction decreases with increasing  $b$  and hence can be made smaller for a larger, more distant mirror.

In classical optics, the effects of diffraction are normally of the order of the wavelength divided by the size of the object. This arises when one is looking at the power in the diffracted wave, which is given by the square of Eq. (49). In our case, there is a possible contribution from an interference term between the diffracted wave and the geometric optics contributions. If a more detailed calculation were to find that this term vanished, then our estimates for  $h^{-2}i$  and  $hE^{-2}i$  would become smaller than Eqs. (50) and (51), respectively, by an additional factor of  $b/a$ .

## 7.2 Edge Effects and Finite Reflectivity

Our model of the mirror is one in which it is not only perfectly reflecting, but also has a sharp edge at which the reflectivity falls discontinuously to zero. Both of these assumptions are oversimplifications to which the singular behavior of  $h'^2 i$  and  $hE^2 i$  may be attributed. Consider the sharp edge assumption. A more realistic model might have the reflectivity falling smoothly to zero over an angular interval of width  $\Delta$  at the edges of the mirror. This would remove the singularities found above at specific values of  $\theta$ . Recall that these singularities arise when an edge of the mirror, at  $\theta = 0$ , sits at an extremum of  $f(\theta)$ . In the case of a smoothed edge, both  $h'^2 i$  and  $hE^2 i$  will be bounded for fixed  $a$

$$jh'^2 i < \frac{1}{a^2} \quad (52)$$

and

$$jhE^2 i < \frac{1}{a^4 (\Delta)^3} : \quad (53)$$

Smoothing of the edges of the mirror is also expected to remove the cusps at  $\theta = \frac{\pi}{2}$ .

The smoothed edges do not, however, remove the singularities as  $a \rightarrow 0$ . This singularity is presumably due to the assumption of perfect reflectivity at all wavelengths. A more realistic model would have the reflectivity go to zero at short wavelengths. Suppose that the mirror becomes transparent for wavelengths less than some minimum value,  $\lambda_m$ . Then we expect to find the bounds

$$jh'^2 i < \frac{1}{\lambda_m^2} \quad (54)$$

and

$$jhE^2 i < \frac{1}{\lambda_m^4} : \quad (55)$$

One reason for reduced reflectivity at short wavelengths is dispersion. The mirror can be regarded as close to perfectly reflecting only for wavelengths longer than about the plasma wavelength  $\lambda_p$  of the metal in the mirror. Thus our results are only valid when  $a > \lambda_p$ . For aluminum, for example,  $\lambda_p \approx 84 \text{ nm}$ . However, it is unlikely that dispersion alone is capable of removing all short distance singularities. The reason for this is that dielectric functions approach unity as  $(\omega = \omega_p)^2$  as  $\omega \rightarrow 0$ . This is not fast enough to regulate integrals which diverge quartically as the short wavelength cutoff. In the case of a plane interface between vacuum and a dispersive material, quantities such as  $hE^2 i$  still diverge as the interface is approached, although less rapidly than in the case of a perfect mirror [2]. Thus it seems that other effects, such as surface roughness, the breakdown of the continuum description at the atomic level, or quantum uncertainty in the location of the interface [3] are needed to produce finite values of  $hE^2 i$ . If any effect does produce a sufficiently sharp cutoff at short wavelengths below about  $\lambda_m$ , then we would have the bounds in Eqs. (54) and (55) even without removing the assumption of a sharp edge to the mirror.

## 8 Observable Consequences

In I, several possible experimental tests of the enhanced vacuum fluctuation near the focus were discussed. Here these tests will be reviewed and further discussed. The most direct test would seem to be to measure the force on an atom or other polarizable particle. In a regime where the atom can be described by a static polarizability  $\alpha$ , the force is  $F = -\nabla V$ , where

$$V = -\frac{1}{2} \hbar E^2 \alpha; \quad (56)$$

In the vicinity of the focus, we have found that

$$\hbar E^2 \alpha = \frac{\beta}{a^4}; \quad (57)$$

where  $\beta$  is a dimensionless constant. For an atom in its ground state, Eq. (56) should be a good approximation when  $a$  is larger than the wavelength associated with the transition to the first excited state.

One might try to measure the deflection of atoms moving parallel to the focal line of a parabolic cylinder. The analogous experiment for a flat plate was performed by Sukenik et al [4] and confirmed Casimir and Polder's theoretical prediction [5]. In the present case, the expected angular deflection is

$$\frac{\Delta \theta}{\theta} = 0.25 \frac{1}{10^3} \frac{m_{Na}}{m} \frac{1}{a} \frac{t^2}{10^3 s} : \quad (58)$$

Here  $m_{Na} = 3.8 \times 10^{-23}$  gm and  $\alpha_{Na} = 3.0 \times 10^{-22}$  cm<sup>3</sup> denote the mass and polarizability of the sodium atom, respectively. (Note that polarizability in the Lorentz-Heaviside which we use is 4 times that in Gaussian units.) If  $t$  is of order  $10^3$  s (the time needed for an atom with a kinetic energy of order 300K to travel a few centimeters), and  $z$  is of order 1 m, the fractional deflection is significant.

An alternative to measuring the deflection of the beam might be to measure the relative phase shift in an atom interferometer, which are sensitive to phase shifts of the order of  $10^4$  radians [6]. If one path of the interferometer were to be parallel to the focal line at a mean distance of  $a$  and the other path far away, the phase difference will be

$$\Delta \phi = \frac{t}{2} \hbar E^2 \alpha = 0.04 \frac{1}{10^3} \frac{m_{Na}}{m} \frac{1}{a} \frac{t}{10^3 s} : \quad (59)$$

Both deflection and phase shift measurements would require the atoms to be rather well collimated and localized near the focal line.

Perhaps the most dramatic confirmation of enhanced vacuum fluctuations would be the trapping of atoms near the focus. This would require a mirror with  $\epsilon_0 > \frac{1}{2}$  so that there is a region with  $\hbar E^2 \alpha > 0$ . It would also require the atoms to be cooled below a temperature of about

$$T_m = 2 \times 10^9 K \frac{1}{10^3} \frac{m_{Na}}{m} \frac{1}{a} : \quad (60)$$

Thus at temperatures of the order of  $10^9$  K, atoms could become trapped in a region of the order of  $1 \mu\text{m}$  from the focus. This type of trapping would be quite different from that currently employed [7] in that it would require no applied classical electromagnetic fields.

## 9 Discussion and Conclusions

In this paper we have further developed a geometric optics approach to the study of vacuum fluctuations near the focus of parabolic mirrors. The main result of this approach is that the mean squared scalar field  $\langle \phi^2 \rangle$  and mean squared electric field  $\langle E^2 \rangle$  grow as inverse powers of  $a$ , the distance from the focus, for small  $a$ . The key justification of geometric optics is its self-consistency. When  $\langle \phi^2 \rangle$  and  $\langle E^2 \rangle$  are large, the dominant contributions must come from short wavelengths for which geometric optics is a good approximation. This was discussed more quantitatively in Sect. 7.

We have given some explicit analytic and numerical results for  $\langle \phi^2 \rangle$  and  $\langle E^2 \rangle$  near the focal line of a parabolic cylindrical mirror. In this paper, we restricted our attention to the case that the angular size of the mirror,  $2\theta_0$ , is less than  $\frac{4}{3}$ . This insures that there are never more than two reflected rays for a given incident ray and simplifies the analysis. We find that for smaller mirrors,  $\theta_0 < \frac{\pi}{2}$ ,  $\langle \phi^2 \rangle > 0$  and  $\langle E^2 \rangle < 0$  everywhere. In this case, an atom will feel a repulsive force away from the focus. For larger mirrors,  $\frac{\pi}{2} < \theta_0 < \frac{2\pi}{3}$ , these mean squared quantities can have either sign, depending upon the direction from the focus. In directions nearly perpendicular to the symmetry axis,  $\theta \approx \frac{\pi}{2}$ , we find  $\langle \phi^2 \rangle < 0$  and  $\langle E^2 \rangle > 0$ . In this case, the force on an atom is attractive toward the focus and trapping becomes a possibility.

In the geometric optics approximation, the mean squared electric and magnetic fields are equal, so the local energy density is equal to  $\langle E^2 \rangle$ . Thus, when  $\langle E^2 \rangle < 0$ , the local energy density is negative, and one has columns of negative energy density running parallel to the focal line of the parabolic cylinder.

The feasibility of experiments to observe the effects on atoms near the focus was discussed in Sect. 8. Although the effects are small, it seems plausible that they could be observed.

**Acknowledgement:** We would like to thank Ken O'Leary for valuable discussions. This work was supported in part by the National Science Foundation under Grant PHY-9800965, by Conselho Nacional de Desenvolvimento Científico e Tecnológico do Brasil (CNPq), and by the U.S. Department of Energy (D.O.E.) under cooperative research agreement DF-FC 02-94ER 40810.

## Appendix

In this Appendix, we will develop a method which goes beyond the geometric optics approximation, and use it to estimate the size of the corrections due to diffraction

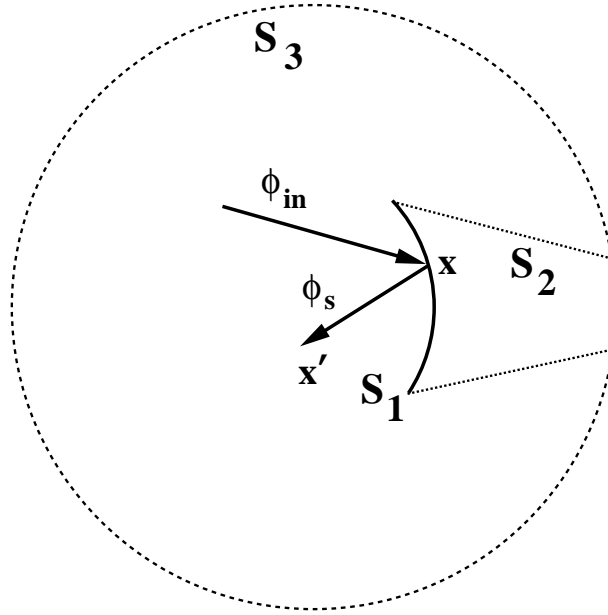


Figure 13: A closed surface  $S$  consists of three parts, the open surface of interest  $S_1$ , a segment  $S_2$  hidden from the view of an observer at  $x^0$ , and a portion  $S_3$  at a very large distance. An incident wave  $\phi_{in}$  reflects from  $S_1$  and produces the scattered wave  $\phi_s$ . Here  $x$  is an arbitrary point in  $S_1$ .

effects. Here we will discuss only a scalar field which satisfies Dirichlet boundary conditions on the mirror. The basic method is to write down and then approximately solve an integral equation for the scattered wave. This method was first used by Kirchhoff to discuss diffraction in classical optics. Let  $\psi(x)$  be a solution of the Helmholtz equation

$$\nabla^2 \psi + k^2 \psi = 0; \quad (61)$$

and let  $G(x; x^0)$  be a Green's function for this equation

$$\nabla^2 G + k^2 G = -\delta(x - x^0); \quad (62)$$

If we multiply Eq. (61) by  $G$ , Eq. (62) by  $\psi$ , take the difference, and integrate over an arbitrary spatial volume  $V$ , the result is

$$\psi(x^0) = \int_S da \cdot [\psi(x) \nabla G(x; x^0) - G(x; x^0) \nabla \psi(x)]; \quad (63)$$

Here  $S$  is the boundary of  $V$ , and  $da$  is outward directed.

We are interested in calculating the scattered wave from a open surface  $S_1$ , rather than the solution on the interior of a closed surface  $S$ . However, we can let the closed surface  $S$  consist of three segments, as illustrated in Fig. 13. The first is the surface of interest  $S_1$ , the second is a segment  $S_2$  which is hidden from the view of

an observer in the region where we wish to find the scattered wave, and the third  $S_3$  closes the surface at a large distance. We now ignore the contributions of  $S_2$  and  $S_3$ , and assume that  $\psi = 0$  on  $S_1$ , so that we have

$$\psi(\mathbf{x}^0) = \int_{S_1}^Z da \, r(\mathbf{x}) G(\mathbf{x}; \mathbf{x}^0) : \quad (64)$$

This is still an integral equation which relates values of  $\psi$  on the surface to those of  $\psi$  of the surface. We can solve it in an approximation in which an incident wave scatters only once from the surface. Let  $\psi_{in}$  be the incident wave, and assume that on  $S_1$

$$\hat{n} \cdot \nabla \psi = 2\hat{n} \cdot \mathbf{k} : \quad (65)$$

We next choose the empty space Green's function

$$G(\mathbf{x}; \mathbf{x}^0) = \frac{e^{ik|\mathbf{x} - \mathbf{x}^0|}}{4|\mathbf{x} - \mathbf{x}^0|} ; \quad (66)$$

and interpret Eq. (64) as giving the scattered wave,  $\psi_s$ ,

$$\psi_s(\mathbf{x}^0) = \int_{S_1}^Z da \, r_{in}(\mathbf{x}) G(\mathbf{x}; \mathbf{x}^0) : \quad (67)$$

The physical interpretation of this expression is that each point on  $S_1$  radiates a scattered wave proportional to  $\hat{n} \cdot \nabla \psi_{in}$ ; the superposition of these individual contributions forms the net scattered wave, as expected from Huygen's principle.

Let the incident wave be a plane wave

$$\psi_{in} = e^{ik \cdot \mathbf{x}} ; \quad (68)$$

and the surface  $S_1$  be the portion of the  $x = 0$  plane in the interval  $-y_0 < y < y_0$ . That is, it is a strip which is infinite in the  $z$ -direction. Take the wavevector of the incident wave to be  $\mathbf{k} = k(\cos \theta; \sin \theta; 0)$  and the observation point to be  $\mathbf{x}^0 = (b; 0; 0)$ , that is, at a distance  $b$  from the mirror, as illustrated in Fig. 14. We can now write the scattered wave as

$$\psi_s(\mathbf{x}^0) = \frac{ik \cos \theta}{2} \int_{-y_0}^{y_0} dy e^{ik \sin \theta y} \int_1^Z dz \frac{e^{ik \sqrt{y^2 + z^2 + b^2}}}{\sqrt{y^2 + z^2 + b^2}} : \quad (69)$$

The  $z$ -integration may be performed explicitly, with the result

$$\psi_s(\mathbf{x}^0) = \frac{1}{2} k \cos \theta \int_{-y_0}^{y_0} dy e^{ik \sin \theta y} H_0^{(1)}(k \sqrt{y^2 + b^2}) ; \quad (70)$$

where  $H_0^{(1)}$  is the Hankel function of the first kind. In general, the remaining integral cannot be evaluated explicitly. However, in the case of an infinite plane mirror,  $y_0 \rightarrow \infty$ , it can be evaluated, with the result

$$\psi_s(\mathbf{x}^0) = e^{ik \sin \theta b} = e^{ik^0 x^0} : \quad (71)$$

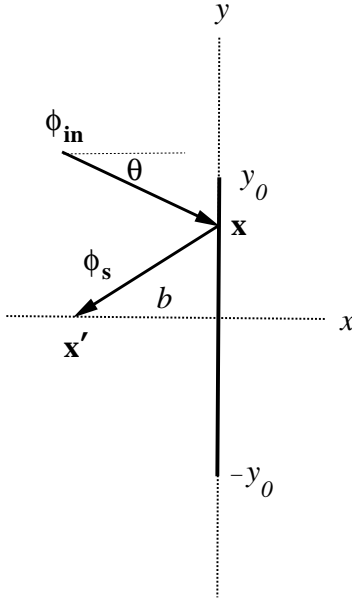


Figure 14: A reflecting strip lies in the interval  $-y_0 < y < y_0$  and is infinite in the  $z$ -direction, normal to the page. A plane wave  $\phi_{in}$  is incident at an angle of  $\theta$  and creates the reflected wave  $\phi_s$  at the point  $x'$ , located a distance  $b$  from the strip.

This is just the result predicted by geometric optics. In the special case of an infinite plane mirror, geometric optics gives the exact result. In the case of a finite mirror, Eq. (71) is still a good approximation in the high frequency limit. In this limit, one may evaluate the integral in Eq. (70) using the stationary phase approximation. So long as the classical path intersects the mirror in the interval  $-y_0 < y < y_0$ , then there is one point of stationary phase within the range of integration. This intersection occurs if  $-y_0 < b \cos \theta < y_0$ . The result of the stationary phase approximation is just Eq. (71), reflecting the fact that geometric optics is a good approximation in the high frequency limit.

Now we wish to give a quantitative estimate of the accuracy of the approximation. Let

$$s = \frac{1}{2} k \cos \theta \int_{-y_0}^{y_0} dy e^{ik \sin \theta y} H_0^{(1)}(k \sqrt{y^2 + b^2}) \quad (72)$$

This is the difference between the stationary phase (geometric optics) approximation and the exact result for a finite mirror, so  $|s| = |j_s - j_{s,j}|$  is a fractional measure of the accuracy of the approximation.

In the high frequency limit that  $k \gg b$ , we can use the large argument form for  $H_0^{(1)}$ ,

$$H_0^{(1)}(z) \sim \frac{e^{i(z - \pi/4)}}{z} \quad (73)$$

and write

$$s \frac{k}{2} \cos \theta \int_{y_0}^{\infty} dy (y^2 + b^2)^{-\frac{1}{4}} e^{ik(\sin \theta y - \sqrt{y^2 + b^2})} + (y_0 \rightarrow -y): \quad (74)$$

The above integral still cannot be evaluated explicitly, but we can estimate it as being of order  $1 = (k \sqrt{y_0})$  when  $k \rightarrow y_0$ . With this estimate, we find that

$$j_{sj} \approx \frac{1}{2} \frac{1}{y_0}; \quad (75)$$

where  $\lambda$  is the wavelength of the incident wave.

## References

- [1] L.H. Ford and N.F. Svaiter, Phys. Rev. A 62, 062105 (2000).
- [2] V. Sopova and L.H. Ford, The Energy Density in the Casimir Effect, quant-ph/0204125.
- [3] L.H. Ford and N.F. Svaiter, Phys. Rev. D 58, 065007 (1998).
- [4] C.I. Sukenik, M.G. Boshier, D.Cho, V. Sandoghar, and E.A. Hindz, Phys. Rev. Lett. 70, 560 (1993).
- [5] H.B.G. Casimir and D. Polder, Phys. Rev. 73, 360 (1948).
- [6] See, for example, C.E. Wineland, D.F. Pritchard, and D.J. Wineland, Rev. Mod. Phys. 71, S253 (1999), and references therein.
- [7] See, for example, W.D. Phillips, Rev. Mod. Phys. 70, 721 (1998), and references therein.